Thermoelectric Properties of p-Type Cu2O, CuO, and NiO from Hybrid Density Functional Theory

Thermoelectric Properties of p-type Cu_2O, CuO, and NiO from Hybrid Density Functional Theory

Jarno Linnera,[†] Giuseppe Sansone,[‡] Lorenzo Maschio,[¶] and Antti J. Karttunen[*,†]

†*Department of Chemistry and Materials Science, Aalto University, Kemistintie 1, 02150 Espoo, Finland*

‡*Dipartimento di Chimica, Università di Torino, Via P. Giuria 5, 10125 Torino, Italy*

¶*Dipartimento di Chimica, C3S centre, NIS centre, Università di Torino, Via P. Giuria 5, 10125 Torino, Italy*

E-mail: antti.j.karttunen@iki.fi

Abstract

The electronic transport coefficients of three Earth-abundant metal oxides Cu_2O, CuO, and NiO were investigated using hybrid density functional theory (DFT). Hybrid DFT methods combined with local Gaussian-type basis sets enabled band structure studies on both non-magnetic and magnetic p-type metal oxides without empirical corrections. CRYSTAL code was used for obtaining the wavefunction and the transport properties were calculated with two different methodologies to benchmark their accuracy: a numerical approach as implemented in the BoltzTraP code and an analytical approach recently implemented in CRYSTAL17. Both computational methods produce identical results in good agreement with experimental measurements of the Seebeck coefficient. The predicted electrical conductivities are overestimated, owing likely to the used approximation of a constant electronic relaxation time in the calculations, as explicit electron scattering is neglected and relaxation time is considered only as a free parameter. The obtained results enable us to critically review and complement the available theoretical and experimental literature on the studied p-type thermoelectric metal oxide materials.

Introduction

The modern world has an ever-growing need for energy due to the increasing population and the constant technological developments. In the case of electricity generation, there is still room for improvement in the efficiency of energy conversion processes. In particular, the majority of the electricity we produce comes from combustion processes, and far too much energy is lost as waste heat in this conversion process. Finding ways to harvest the waste heat has become a major goal, not only from the economic perspective but also from the sustainability point of view as well.[1] One option is to convert the waste heat to electricity by utilizing the thermoelectric Seebeck effect. All materials show the Seebeck effect, but for most compounds, the magnitude of the effect is small or negligible. The thermoelectric

efficiency is described by the dimensionless figure-of-merit zT, which can be calculated from three fundamental material parameters as $zT = \sigma S^2 T/\kappa$, where σ, S, and κ are the electrical conductivity, Seebeck coefficient, and thermal conductivity, respectively.

Naively, one should just pursue materials with high Seebeck coefficient and electrical conductivity accompanied by a low thermal conductivity. Unfortunately, materials with high electrical conductivity often conduct heat equally as well, as is the case for metals where electrons carry also the majority of the heat. Decoupling the conductivities in practice is far from trivial.[2] This can, however, to some degree be achieved by considering κ as a sum of electronic and phononic thermal conductivity and focusing on semiconductors and insulators. In such materials, the majority of the heat is carried by phonons. With an increasing band gap, the electrons carry less and less heat, and with e.g. nanostructuring or other means of structural manipulation, the flow of phonons can be suppressed without lowering the electronic conductivity too much.[3] With appropriate doping, the electronic properties can even be enhanced along the suppression of thermal conductivity.

Even if we had a robust method to improve the thermoelectric efficiency, we still need a suitable starting material to apply them to. Currently, some of the best thermoelectric materials include, for example, simple tellurides such as Bi_2Te_3 or PbTe, that have been improved via various degrees of doping to have zT values high enough for applications.[4–6] These examples are unsuitable for mass production, however, owing to the toxicity of lead and the scarcity of tellurium. Increasing amount of effort has gone to finding well performing thermoelectric materials containing only non-toxic and abundant elements.[7] This has lead to shifting focus towards different compound groups such as sulfides, e.g. CuS, as well as oxides, e.g. ZnO, Cu_2O, and SnO.[8–14]

In stoichiometric bulk form, transition metal oxides have inherently too low zT values for any commercial use. Using the previously mentioned techniques, the thermoelectric performance of oxide materials has slowly increased over the years. The first major improvement in n-type materials was seen in the work of Ohtaki *et al.*, where ZnO was doped with 2%

of Al and a zT of 0.30 at 1000 K was measured, a value much higher than for any other contemporary oxide material.[15] This was later on improved further by doping it also with 2% gallium, increasing zT to 0.47 at 1000 K. Other means of thermoelectric engineering of zinc oxide include decreasing thermal conductivity by creating an inorganic-organic superlattice, which increases phonon scattering.[16–18]

Another early highlight was the discovery of $NaCo_2O_4$ as a possible p-type thermoelectric material, which sparked a lot of interest in layered structures.[19,20] Numerous other cobalt oxides were studied soon after, but a major breakthrough for such oxides is yet to be seen. Layered structures are in general an attractive group of compounds, as they provide a convenient platform for nanostructuring through intercalation, and different stoichiometries can be rather easily explored by altering the synthesis conditions.[21,22]

As with many other fields of chemistry, computational methods are nowadays a key element in design and discovery of thermoelectric materials.[23,24] Along with providing a rationale to the outstanding performance of some material groups, the possibility to find trends and engineer the band structure before even synthesizing the materials can significantly speed up the process of finding suitable compositions for wider use.[25,26] All three parameters needed to evaluate the zT of a material can be calculated with quantum chemical methods to a fairly accurate degree. Seebeck coefficient can be obtained rather straightforwardly within the rigid band and constant electron relaxation-time (RT) approximations. With the same approximations, the electrical conductivity and the electronic part of the thermal conductivity can be obtained with respect to the relaxation time, which must be either set as an empirical parameter or obtained from more elaborate first-principles calculations (*vide infra*). The minimal input required for these calculations is only the band structure with a dense k-mesh in the reciprocal space, a rather trivial effort with modern computational capacity. The lattice thermal conductivity can also be obtained from first-principles calculations by means of lattice dynamics and Boltzmann transport theory.[27]

In this paper, we apply hybrid density functional methods to investigate the thermoelec-

tric properties of three p-type semiconductor oxides composed of Earth-abundant elements: Cu_2O, CuO, and NiO (Figure 1). We will first recap the main theoretical and computational aspects, then discuss the structural details and the band structures of the materials, followed by analysis of transport properties. We solve the transport coefficients of the materials both numerically using BoltzTraP and analytically using a novel method implemented in CRYSTAL17 by some of the present authors.[28,29] This allows us to provide a thorough comparison of the two computational strategies for both non-magnetic (Cu_2O) and magnetic (CuO and NiO) materials.

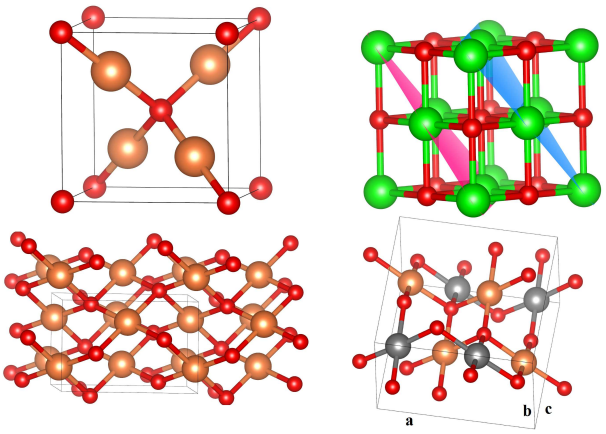

Figure 1: Unit cells and magnetic structures of the studied materials. Top left: Crystal structure of Cu_2O. Brown, Cu; Red, O. Top right: Crystal structure of NiO. Colored planes mark the adjacent [111] planes where the nickel atoms have different spins. Green, Ni; Red, O. Bottom left: Crystal structure of CuO. Brown, Cu; Red, O. Bottom right: Magnetic structure of CuO. Brown, Cu spin up; Silver, Cu spin down; Red, O.

General theory and methodology

Calculation of the transport coefficients

Boltzmann theory of transport has been covered in many textbooks, e.g. by Ziman.[30] Here we summarize only some fundamental aspects required to follow the discussion of the results obtained from BoltzTraP[28] and CRYSTAL17.[29] The definitions below are given using atomic units.

In its simplified semiclassical form without a magnetic field, Boltzmann transport equation describes the electrical current in a material that is subjected to an electric field E_b and a thermal gradient ∇_b as

$$j_a = \sigma_{ab} E_b + \nu_{ab} \nabla_b T + ... \ . \tag{1}$$

Prefactors of the electric field and thermal gradient are the conductivity tensors, that can be obtained by integrating the conductivity distributions, written with tensors of Eq. 7 below as

$$\sigma_{qr}(T;\mu) = \int \Xi_{qr}(\epsilon) \left[-\frac{\partial f_\mu(T;\epsilon)}{\partial \epsilon} \right] d\epsilon, \tag{2}$$

$$\nu_{qr}(T;\mu) = \frac{1}{T} \int \Xi_{qr}(\epsilon) \left[-\frac{\partial f_\mu(T;\epsilon)}{\partial \epsilon} \right] (\epsilon - \mu) d\epsilon, \tag{3}$$

$$\kappa^0_{qr}(T;\mu) = \frac{1}{T} \int \Xi_{qr}(\epsilon) \left[-\frac{\partial f_\mu(T;\epsilon)}{\partial \epsilon} \right] (\epsilon - \mu)^2 d\epsilon, \tag{4}$$

where $\kappa^0_{qr}(T;\mu)$ is the electronic contribution to the thermal conductivity. Using the transport tensors, the Seebeck coefficient can be written as

$$S_{ab} = E_a (\nabla_b T)^{-1} = (\sigma^{-1})_{qa} \nu_{qb}. \tag{5}$$

The transport distribution function $\Xi_{qr}(\epsilon)$ is defined for band index i and reciprocal space vector $\mathbf{k}$ as

$$\Xi_{qr}(i,\mathbf{k}) = \tau_{i,\mathbf{k}} v_q(i,\mathbf{k}) v_r(i,\mathbf{k}), \tag{6}$$

where $v_q(i,\mathbf{k})$ and $v_r(i,\mathbf{k})$ are the group velocities and $\tau_{i,\mathbf{k}}$ is the electronic relaxation time. For practical calculations, it is easier to define the energy projected tensor

$$\Xi_{qr}(\epsilon) = \frac{1}{N} \sum_{i,\mathbf{k}} \sigma_{qr}(i,\mathbf{k}) \delta(\epsilon - \epsilon_{i,\mathbf{k}}), \tag{7}$$

where N is the number of $\mathbf{k}$-points used in sampling the reciprocal space. In Eq. 7 $\delta(x)$ is Dirac's delta function or – more commonly – an approximation to it that involves some broadening (*e.g.* Gaussian broadening).

It is clear from the above that the most challenging computational task, from an *ab initio* perspective, is the determination of the band velocities

$$v_{i,q}(\mathbf{k}) = \frac{\partial \epsilon_{i,k}}{\partial k_q} \tag{8}$$

where k_q is the component of the $\mathbf{k}$ vector along the cartesian direction q. Such derivative can be performed either analytically or numerically. In the BoltzTraP program[28] the bands are interpolated based on symmetry adapted planewaves that are, then, used to estimate the derivative in Eq. 8. In CRYSTAL17 the locality of the atom-centered basis functions adopted is exploited allowing for the evaluation of such derivatives in a simple and straightforward way.[29,31] A similar approach, but based on the localization of the wavefunction, is adopted in the BoltzWann code[32] that was not used in this work.

The tensors in Eqs. 2 – 4 can be cast as a function of carrier concentration, rather than chemical potential, which allows an easier comparison with the experimental data. This is achieved through the calculation of the temperature-dependent number of carriers $N_{\mu,T}$:

$$N_{\mu,T} = \frac{n}{N_{\mathbf{k}}} \sum_{\mathbf{k}} \sum_{i} \frac{1}{exp\left(\frac{\epsilon_i(\mathbf{k})-\mu}{k_B T}\right) + 1} \tag{9}$$

the Fermi-Dirac distribution has been used, n is the number of electrons per state and $N_{\mathbf{k}}$ is the number of k-points in the irreducible Brillouin zone. The carrier concentration $\rho(\mu)$ is obtained for a given temperature T as:

$$\rho(\mu) = \frac{N_\mu}{V} \tag{10}$$

where V is the unit cell volume.

As mentioned in the Introduction, calculation of the various thermoelectric properties is straightforward within the RT approximation. It makes the critical assumption that $\tau_{i,\mathbf{k}}$ is independent of the band index i and the $\mathbf{k}$-vector direction, although it is obviously not. This was shown also by some recent, more accurate calculations.[33] Computing the electronic relaxation times *ab initio* is a formidable task as it requires explicit information on the electron-phonon (e-ph) scattering. Quite some effort has been put to developing techniques that make e-ph interactions computationally tractable.[34,35] When calculating the e-ph matrix elements, the convergence with respect to $\mathbf{q}$-points in the Brillouin zone is extremely slow, and the sheer number of needed calculations still hinders the more complete solution of becoming standard procedure, especially for high-throughput screening purposes.

Computational details

All DFT calculations were performed with CRYSTAL14 and CRYSTAL17 program packages.[36,37] All presented results were obtained using the hybrid PBE0 functional in conjunction with all-electron, triple-ζ-valence + polarization level Gaussian-type basis sets based on Karlsruhe def2 basis sets (detailed basis set listings are provided in the Supporting Information).[38–40] For all structures, the convergence with respect to k-points in the reciprocal space was checked. The used meshes were $8 \times 8 \times 8$ for Cu_2O and NiO, and $4 \times 8 \times 4$ for CuO. The TOLINTEG parameters, controlling the tolerance factors for the Coulomb and exchange integrals, were set to 8, 8, 8, 8 and 16. We used the default integration grid (XLGRID) in all CRYSTAL calculations for the density functional part, along with the default total energy convergence threshold in the geometry optimization (TOLDEE). The optimized geometries together with the ground state spin configurations are provided in the Supporting Information. Wavefunctions from CRYSTAL14 were used to create inputs for BoltzTraP calculations.[28] We raised TOLDEE to 10^{-9} a.u. to calculate a more accurate wavefunction at the optimized geometry for BoltzTraP. The same energy convergence criterion value was used when the structures were checked for being true local minima by calculating the vibra-

tional frequencies at the Γ-point. For BoltzTrap, the wavefunctions were recalculated at a much denser k-mesh than what was used in the optimizations, 48 × 48 × 48 for Cu_2O and NiO, and 30 × 40 × 30 for CuO. In the BoltzTraP calculations,the number of interpolated lattice points per k-point (LPFAC) was set to five.

Results and discussion

Geometries and electronic properties

The studied oxides have very different structures. Cu_2O crystallizes in the cubic $Pn\bar{3}m$ space group. One unit cell, shown in Figure 1, consists of two formula units. All oxygen atoms are surrounded by copper atoms in a perfect tetrahedral coordination, the Cu atoms being linearly coordinated to two oxygen atoms. Unlike NiO and CuO, in Cu_2O the metal has a filled d-shell and the material is thus non-magnetic. The initial lattice parameter a was taken from a synchrotron radiation study by Kirfel and Eichhorn.[41]

The structure of CuO is a bit more complicated. It crystallizes in the monoclinic Cc space group and the structure consists of zig-zagging CuO_4 square planes, where the oxygen atoms form distorted tetrahedra with copper, as shown in Figure 1. Cu(II) has an unpaired electron and CuO has an antiferromagnetic ground state below the Néel temperature of 230 K.[42] For the magnetic structure, a supercell with new lattice vectors $\mathbf{a}' = \mathbf{a} + \mathbf{c}$, $\mathbf{b}' = \mathbf{b}$ and $\mathbf{c}' = -\mathbf{a} + \mathbf{c}$ was created and spins were assigned similar to a previous computational study by Rödl *et al.*, shown in Figure 1.[43] Initial lattice parameters were taken from an x-ray study by Åsbrink and Waskowska.[44]

NiO, on the other hand, has a simple face-centered cubic crystal structure ($Fm\bar{3}m$), where all atoms are surrounded by the other species in perfect octahedral coordination. However, due to the d^9 electron configuration, NiO has a slightly more complex antiferromagnetic ground state in temperatures below the Néel temperature (525 K).[45] In the experimentally found AF_2 structure, the nickel atoms with opposite spin are arranged in adjacent [111]

sheets (Figure 1). In the calculations this was accomplished by constructing a supercell from the primitive lattice vectors using new lattice parameters **a**' = **b** + **c**, **b**' = **a** + **c** and **c**' = **a** + **b**. The initial lattice parameter a for the FCC unit cell was taken from an X-ray study by Sasaki *et al.*[46]

Geometry optimizations at DFT-PBE0/TZVP level of theory resulted only in minor changes in the lattice parameters and atomic positions compared to the initial experimental values. Table 1 shows all the optimized lattice parameters and the relative change compared to the experimental structure is shown in parentheses (lattice parameters and atom positions in CRYSTAL input format are found in the Supporting Information). All lattice vectors elongated slightly during the optimization. Using the correct magnetic structures is paramount in the calculations, as the ground state is predicted to be metallic for both NiO and CuO without the correct antiferromagnetic spin configurations. Magnetic moments of the metal atoms given by PBE0 agree well with experimental measurements. The calculated spin-only magnetic moment of the Ni atoms is 1.67 μ_B, compared to the experimental full magnetic moment of 1.90 μ_B.[47] It is known from experiment and calculations that orbital momentum plays some role in the full magnetization density of NiO, thus improving the comparison between our results and experiments as we do not consider spin-orbit coupling in the calculations.[48,49] For CuO our calculations produce a spin moment of 0.64 μ_B for the Cu atoms, while the experimental values for the atomic magnetic moments are rounded to 0.68 μ_B.[50,51]

Figure 2 shows the band structures and DOS plots for all three systems calculated at the PBE0/TZVP level of theory. For Cu_2O, the band gap is in good agreement with earlier experimental results, considering that hybrid functionals have a tendency to overestimate the band gap of insulating and semiconducting materials. The calculated gap is 2.39 eV while the experiments give results varying from 2.0 to 2.2 eV, most often cited value being 2.17 eV.[52,53] The use of hybrid functionals is rationalized with the more accurate description of the electronic structure it provides. In fact, the presence of a fraction of Hartree–Fock like exact

Table 1: Optimized lattice parameters of Cu_2O, NiO and CuO at the PBE0/TZVP level of theory. Difference to the experimental values is shown in parentheses.[a]

Species	a	b	c	β
Cu_2O	4.32 (+1.2 %)	-	-	-
NiO	4.19 (+0.2 %)	-	-	-
CuO	4.73 (+1.1 %)	3.43 (+0.3 %)	5.15 (+0.4 %)	99.7 (+0.3 %)

[a] Geometry optimizations for NiO and CuO were done using supercells described in the text to incorporate the correct spin configuration. The tabulated NiO and CuO cell parameters are obtained by transforming the supercell back to the original crystallographic cell.

exchange acts in reducing, and eventually neutralizing, the self-interaction errors inherent in the DFT approach. This is particularly important in magnetic systems since it favours the spatial localization of the unpaired electrons. Not only is the agreement of the band gap compared to experiments worse using a GGA functional, say PBE, it has been shown to heavily affect other predicted properties as well, such as lattice thermal conductivity.[54]

At first glance, the band gap for CuO seems to be too large open when compared to the often cited values for the experimental band gap. The PBE0/TZVP calculation results in a gap of 3.8 eV, while reports for the experimental gap have varied from 1.0 to 1.9 eV and other theoretical predictions go from metallic to 4.1 eV depending on the used methods.[43,55–60] In this view, the *GW* study by Rödl *et al.* is of particular interest where the band gap increased, not only with the fraction of exact exchange used but also with the level of the used *GW* approximation up to 4.1 eV with the self-consistent G_nW_n, where both the Green's function G and the screened Coulomb interaction W are calculated again with the new eigenvalues at each self-consistency step n until convergence is reached. When the valence bands for Cu_2O and CuO are compared (Figure 2), there is a notable difference in the relative amount of oxygen states. Cu_2O has only some very minor contributions from O states until -5 eV from the valence band maximum, whereas for CuO the states until around -1.5 eV below the valence band maximum are in fact dominated by the O states. As also noted in a recent study, it is consistent with the higher oxidation state lowering the energy of the *d*-states due

to reduced Coulomb repulsion.[61]

For NiO, the experimental band gap lies between 4.0 and 4.3 eV, while in the calculations done here it is as large as 5.3 eV.[62,63] This is in line with the previous results by Moreira *et al.*, where they showed that, again, increasing the amount of exact exchange in the density functional approximation widens the band gap.[64] From the atom-projected DOS, it can be seen that the electronic structure of both Cu(II) and Ni(II) oxides are somewhat similar in the sense that the topmost valence bands consist equally of metal and oxygen states and bands lower in energy have more contribution from the metal.

Transport coefficients of Cu_2O, CuO and NiO

We investigated the Seebeck coefficient S, electrical conductivity σ calculated with the electronic relaxation time as a free parameter ($\sigma/\tau_{i,\mathbf{k}}$), and the power factor $S^2\sigma$ with respect to carrier concentration ρ at a temperature of 600 K for both p-type and n-type carriers. The temperature in the plots shown below was chosen as to represent the performance of some high-T heat-harvesting application at a possible operating temperature. In addition, calculations were done also at several other temperatures corresponding to experiments in order to make reasonable comparisons. We carried out the transport coefficient calculations numerically with BoltzTraP and analytically with CRYSTAL17 to compare the results of these two computational approaches. All the calculated transport coefficients agree perfectly with each other, to the extent that the results are not actually distinguishable from each other. Since all three oxides show similar behavior, CRYSTAL17/BoltzTraP comparisons are shown only for Cu_2O, while the corresponding comparisons for CuO and NiO are shown only in the Supporting Information. The plots for CuO and NiO in the main text show the results from analytical CRYSTAL17 calculations only.

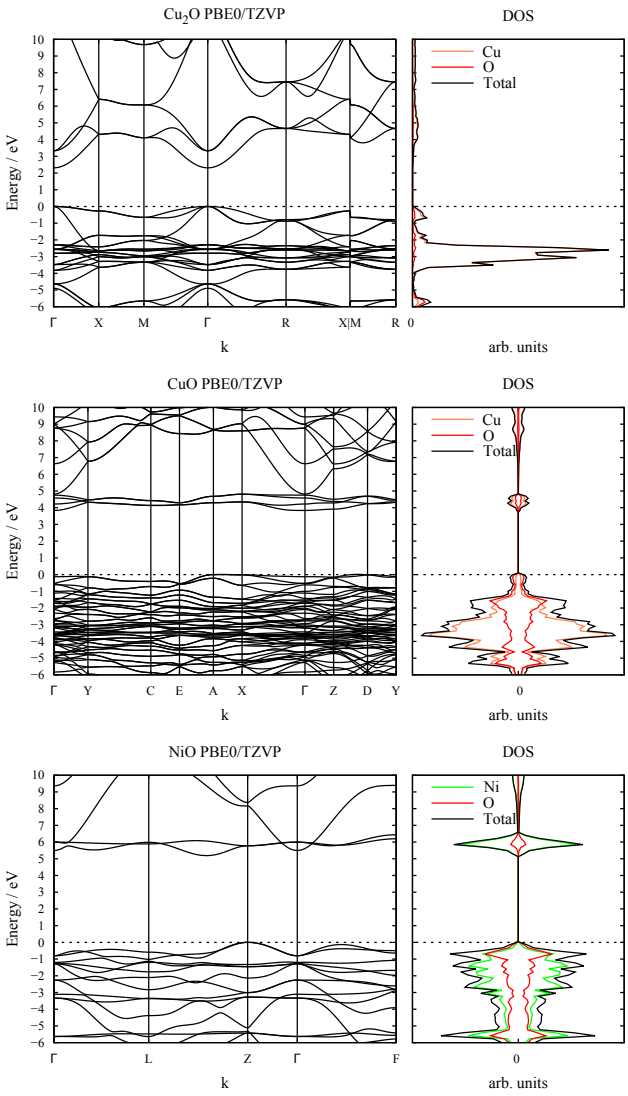

Figure 2: Band structures and atom-projected density of states for the studied materials at the PBE0/TZVP level of theory. For CuO and NiO, the left side of the DOS plot shows the spin down states and right side shows the spin up states. Dashed line marks the valence band maximum, which is set to zero energy. The band paths in the first Brillouin zone have been taken from Ref.[65].

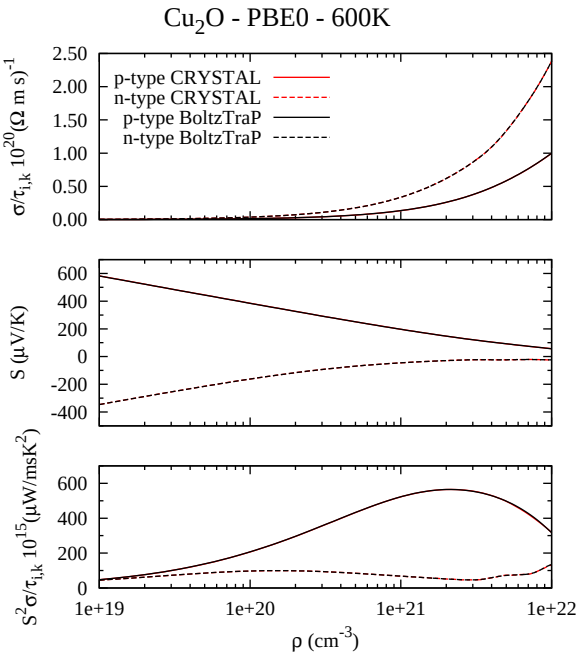

Figure 3: Transport coefficients for Cu_2O as a function of carrier concentration ρ. Top: Electrical conductivity calculated with the electronic relaxation time as a free parameter. Middle: Seebeck coefficient. Bottom: Power factor $S^2\sigma$.

Transport coefficients of Cu_2O

The first measurements of the transport coefficients of Cu_2O date back more than 100 years.[66] Since then they have been re-evaluated through the years and Seebeck coefficient values have reached as high as 1700 µV/K, but the average values settle around 800 µV/K, depending on the measurement temperature and crystal growth characteristics.[67–69]. Our predictions (Figure 3) compare well with the experimental results, although direct comparisons of all properties are difficult since most single crystal studies do not report both hole concentration and Seebeck coefficients. In the single crystal study of Young and Schwartz, they estimated the hole concentration at 500 K to be between 8.5×10^{16} and $2.5\ \times10^{17}$ cm^{-3}, and the measured Seebeck coefficient was around 1050 µV/K.[70] Our calculations using $T = 500$ K predict $S = 970$ µV/K at the lower estimated hole concentration and $S = 870$ µV/K for the higher concentration.

When we compare our predictions against the more recent thin film study by Hartung

et al., our values differ considerably. The experimental Seebeck coefficients are much lower than our theoretical predictions. Our calculations with $T = 300$ K at hole concentration of 3×10^{15} cm^{-3} predict a thermopower of 1200 µV/K whereas their measurements reach around 900 µV/K.[71] They do mention in the paper, however, that their values on the hole concentration should be taken with a grain of salt as the assumption of diffusive transport might not hold. Additionally, the phase purity of the thin film samples will surely not match the perfect Cu_2O crystal we have in our calculations. Another thin film study by Figueira *et al.* reaches Seebeck values close to 1000 µV/K in room temperature and their Hall measurements indicate a carrier concentration of 4×10^{16} cm^{-3}.[72] These results match our calculations almost perfectly, at 300 K our predicted Seebeck with the same concentration is 970 µV/K.

The earlier Cu_2O computational study by Chen *et al.* reports a Seebeck coefficient of slightly over 500 µV/K at a hole concentration of 1×10^{19} cm^{-3}, while our calculations give 580 µV/K at 600 K. One major difference is that they used the GGA-PBE functional whereas we have used the hybrid PBE0 functional. All other parameters for the calculations are the same or do not change the results, e.g. we also did the calculations with the same (less dense) **k**-mesh as Chen *et al.* and found no difference. As the only input for the transport coefficient calculations is the DFT band energies, the differences in the PBE and PBE0 band energies are clearly reflected in the thermopower.

Our calculated *p*-type electrical conductivities are half of that what Chen *et al.* obtained using the PBE-GGA functional. At 300 K their electrical conductivity with respect to electronic relaxation time at a carrier concentration of 1.5×10^{21} cm^{-3} is 4×10^{19} $(\Omega\text{ms})^{-1}$ and we have 2×10^{19} $(\Omega\text{ms})^{-1}$. Similarly, at 500 K they obtained $\sigma/\tau_{i,\mathbf{k}}$ of roughly 5.5 $\times 10^{19}$ $(\Omega\text{ms})^{-1}$ where we have 2.7×10^{19} $(\Omega\text{ms})^{-1}$. The usual conductivity values in experiments span a few orders of magnitude roughly from 1 to 0.01 $(\Omega\text{m})^{-1}$, which are clearly smaller than the conductivities shown in Figure 3 if we set the electronic relaxation time as a parameter.[68,70–74] If we take the same value for ρ as in the results of Figueira

et al., considerably lower than what the calculations suggest for optimized power factor, our electrical conductivity with $\tau_{i,\mathbf{k}}$ as a free parameter is 6.0 $\times$ 10^{14} $(\Omega\mathrm{ms})^{-1}$. Setting the electronic relaxation time to a typical value of 1 fs, we have an electrical conductivity of 0.6 $(\Omega\mathrm{m})^{-1}$, whereas Figueira *et al.* measured 3 $(\Omega\mathrm{m})^{-1}$ at room temperature.

Chen *et al.* report a maximum power factor 350 $\times$ 10^{15} µW/msK^2 at a temperature of 500 K while our value is 440 $\times$ 10^{15} µW/msK^2 with the electrical relaxation time $\tau_{i,\mathbf{k}}$ as a free parameter. Even though our calculated electrical conductivities are halved when compared to the PBE-GGA study, the larger Seebeck coefficient plays a bigger role at smaller values. As the thermoelectric performance is directly proportional to the power factor, based on these results Cu_2O seems even more applicable than what Chen *et al.* had estimated. It is also worth noticing that in their study the maximum of the power factor shifts towards higher carrier concentrations with increasing temperature. As the Seebeck coefficient increases with temperature, the larger relative decrease of S resulting from higher carrier concentrations, and the decline of the power factor, happens later. In reality, the relationship is not so simple, however, as higher carrier concentrations also affect the mobility and scattering times negatively, so the maximum is most likely found at lower ρ than what constant relaxation time approach predicts.

Transport coefficients of CuO

Experimental results for the transport coefficients of stoichiometric CuO are rather scarce, most likely owing to the smaller stability window of CuO compared to Cu_2O at elevated temperatures. In the study of Jeong and Choi, the pressed CuO pellets had a thermopower between 500 and 600 µV/K at the temperature of 600 K.[75] Our results, shown in Figure 4, would match reasonably well with their results if their carrier concentration would be between 1 to 3 $\times$ 10^{19} cm^{-3}. Jeong and Choi estimated ρ = 1 $\times$ 10^{20} cm^{-3} based on the atomic density of copper in their CuO samples. Assuming that the electronic relaxation time is in the order of femtoseconds, our single-crystal calculations within the RT approximation

would result in a clearly larger electrical conductivity than Jeong and Choi obtained for the CuO pellets. We obtain $\sigma = 1.5 \times 10^3$ $(\Omega\ \mathrm{m})^{-1}$ with $\tau_{i,\mathbf{k}} = 1$ fs, while the CuO pellets had $\sigma = 0.5$ $(\Omega\ \mathrm{m})^{-1}$.

Hartung *et al.* report values for the Seebeck coefficient and electrical conductivity similar to Jeong and Choi, $S = 550$ μV/K and $\sigma = 0.3$ $(\Omega\ \mathrm{m})^{-1}$, but their measurements indicate more than two orders of magnitude lower hole concentrations, roughly 2×10^{17} cm^{-3}.[71] This would bring the conductivities better in line with our RT approximation results as we obtain for this hole concentration $\sigma = 4.1$ $(\Omega\ \mathrm{m})^{-1}$ using $\tau_{i,\mathbf{k}} = 1$ fs, although our Seebeck coefficient would then be rather heavily overestimated with $S = 860$ μV/K at the temperature of 300 K. With the same ρ as in the Jeong and Choi's single crystal study Hartung *et al.* have a Seebeck coefficient of 300 μV/K when we have 330 μV/K, and higher concentrations up to 1×10^{21} cm^{-3} bring S down to around 200 μV/K for the thin film study and 135 μV/K for the theoretical results, both at a temperature of 300 K.

The power factor of CuO thin films in the measurements of Hartung *et al.* reaches slightly over 2 μW/mK^2 at room temperature while in the study of Figueira *et al.* the best performing CuO films have a power factor of only 0.5 μW/mK^2. In comparison, the theoretical maximum at 300 K for single crystal CuO (with $\tau_{i,\mathbf{k}} = 1$ fs) is over 300 μW/mK^2 at a carrier concentration of 6×10^{20} cm^{-3}. Here the large difference probably arises both from the single-crystal vs. polycrystalline comparison and the possible overestimations in our $\sigma/\tau_{i,\mathbf{k}}$ values.

Transport coefficients of NiO

As a textbook example of a strongly-correlated d-metal oxide, electrical properties of nickel(II) oxide have been studied extensively over the years. The theoretical results around the power factor optimum at the temperature of 600 K are plotted in Figure 5. The experimental Seebeck coefficient for single crystal NiO with near-perfect stoichiometry is roughly 900 μV/K at the temperature of 600 K, as recommended by Keem and Honig in their comprehensive

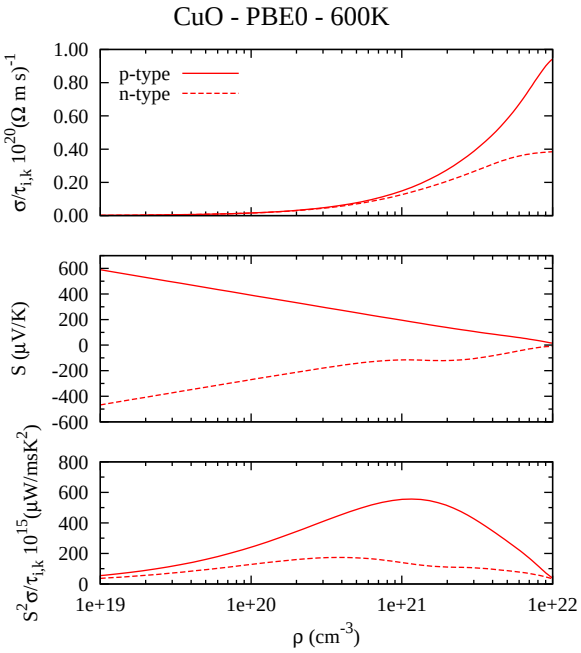

Figure 4: Transport coefficients for CuO as a function of carrier concentration ρ. Top: Electrical conductivity calculated with respect to electronic relaxation time. Middle: Seebeck coefficient. Bottom: Power factor $S^2\sigma$ with respect electronic relaxation time.

review.[76] Such high thermopower would indicate a rather low hole concentration, and low values seem reasonable, considering how the carrier concentration in naturally occurring semiconductors is mostly due to defects and deviation from perfect stoichiometry. Naturally, the electrical conductivity varies strongly between samples of different quality. At the temperature of 600 K, Keem and Honig cite values for σ ranging over six orders of magnitude from 5×10^{-4} to 25 $(\Omega\ \mathrm{m})^{-1}$, not taking into account polycrystalline samples.

For a 900 µV/K thermopower, our calculations predict a carrier concentration of roughly 9×10^{16} cm^{-3} and $\sigma/\tau_{i,\mathbf{k}}$ of 2×10^{15} $(\Omega\ \mathrm{m\ s}\ )^{-1}$. It is rather safe to estimate that when the Seebeck coefficient is as high as 900 µV/K, the electrical conductivity is more likely to be found near the lower end of the experimental results. Only few previous studies mentioned in Keem's review give estimates of the hole concentration. Parravano calculated $\rho = 1 \times 10^{21}$ cm^{-3} at 600 K based on the measured Fermi level and the number of energy levels from the atomic density of nickel in NiO.[77] The study reports a thermopower of 450 µV/K while our calculations predict only 130 µV/K at such high values of ρ. It is a similar situation to CuO,

where carrier concentration seems to be overestimated by the total level density calculation. In another study, Nachman *et al.* measured a thermopower of 600 µV/K at slightly over 600 K.[78] They determined a hole concentration of 2.18 × 10 ^{18} cm^{-3} based on the jodometric titration of Ni(III) in the sample closest to perfect stoichiometry at a temperature of 300 K, which did not change when performed at 340 K. The same sample showed an electrical conductivity of roughly 5 (Ω m)$^{-1}$ at 600 K and the calculations predict $\sigma/\tau_{i,\mathbf{k}} = 100 \times 10^{15}$ (Ω m s)$^{-1}$, a twentyfold overestimation with the example value $\tau_{i,\mathbf{k}} = 1$ fs. It is less than in the case of CuO, but still rather large.

The power factor of pure NiO is rarely the focus of experimental studies as it is far too low for practical applications, owing to the very low electrical conductivity for a TE material. Shin *et al.* measured a power factor of 0.1 µW/mK^2 at a temperature of 650 K.[79] The measured sample had a thermopower of 450 µV/K which according to calculations would indicate a carrier concentration of 2 × 10^{19} cm^{-3}. The corresponding $\sigma/\tau_{i,\mathbf{k}}$ is 4.3 × 10^{17} (Ω m s)$^{-1}$, and if we use the example value $\tau_{i,\mathbf{k}} = 1$ fs, the resulting power factor is 190 µW/mK^2, an overestimation like in the case of CuO.

Conclusions

We have performed hybrid density functional theory calculations on three Earth-abundant transition metal oxide materials and assessed their thermoelectric transport coefficients using a BTE methodology based on analytical derivatives of electronic bands implemented in CRYSTAL17. The results obtained are in excellent agreement with those obtained by the BoltzTrap code starting from the same CRYSTAL wavefunction.

The calculated Seebeck coefficients agree well with the experimental measurements, but the electrical conductivity is clearly overestimated for CuO and NiO. The poorer predictive performance for σ is to be expected as constant relaxation time approximation does not affect the thermopower calculation as strongly as it does the conductivity calculations. Because

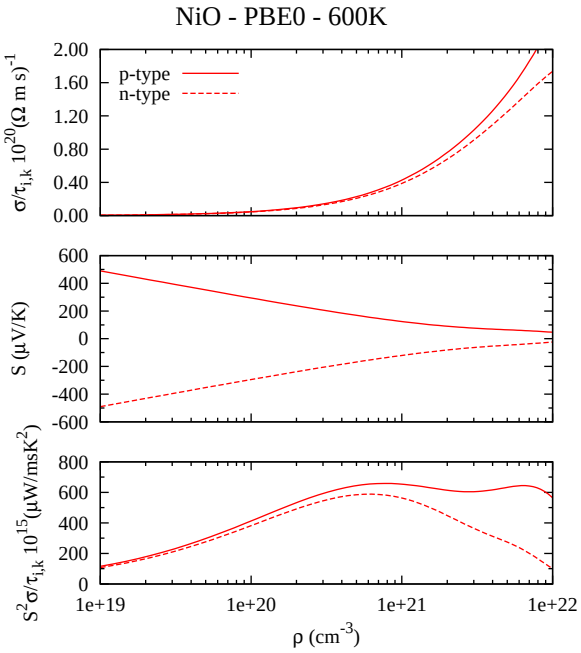

Figure 5: Transport coefficients for NiO as a function of carrier concentration ρ. Top: Electrical conductivity calculated with respect to electronic relaxation time. Middle: Seebeck coefficient. Bottom: Power factor $S^2\sigma$ with respect electronic relaxation time.

the relaxation times could not be obtained from first-principles calculations, the predicted conductivities can only be used as ballpark estimates rather than absolute values. There is a clear need for high-efficiency and high-accuracy methods of predicting the electronic relaxation times of transition metal oxides in conjunction with hybrid DFT methods.

From an electronic point of view Cu_2O, CuO, and NiO show very similar theoretical maximum TE performance within the constant relaxation approximation. In improving the electrical conductivities of NiO and CuO, suitable doping plays a key role. For example, the power factor of NiO at 650 K has been improved three orders of magnitude by 2.4% addition of lithium alone, and there is still room for improvement.[79] Hence, the thermoelectric properties of these relatively simple p-type oxides composed of Earth-abundant elements are encouraging their further enhancement by doping and nanostructuring.

Supporting Information description

Additional computational details, CRYSTAL/BoltzTraP comparison of transport coefficients for NiO and CuO, optimized geometries and ground state spin configurations of the studied materials.

Acknowledgement

The work has been funded by the Academy of Finland (Strategic Research Council, CloseLoop consortium, grant 303452). Computational resources were provided by CSC, the Finnish IT Center for Science.

References

(1) Snyder, G. J.; Toberer, E. S. Complex Thermoelectric Materials. *Nat. Mater* **2008**, *7*, 105–114.

(2) Yang, J.; Yip, H.; Jen, A. K. Rational Design of Advanced Thermoelectric Materials. *Advanced Energy Materials* **2013**, *3*, 549–565.

(3) Biswas, K.; He, J.; Blum, I. D.; Wu, C.-I.; Hogan, T. P.; Seidman, D. N.; Dravid, V. P.; Kanatzidis, M. G. High-performance Bulk Thermoelectrics With All-Scale Hierarchical Architectures. *Nature* **2012**, *489*, 414 – 418.

(4) Poudel, B.; Hao, Q.; Ma, Y.; Lan, Y.; Minnich, A.; Yu, B.; Yan, X.; Wang, D.; Muto, A.; Vashaee, D. et al. High-Thermoelectric Performance of Nanostructured Bismuth Antimony Telluride Bulk Alloys. *Science* **2008**, *320*, 634–638.

(5) Xie, W.; Tang, X.; Yan, Y.; Zhang, Q.; Tritt, T. M. Unique Nanostructures and Enhanced Thermoelectric Performance of Melt-Spun BiSbTe Alloys. *Appl. Phys. Lett.* **2009**, *94*, 102111–1–3.

(6) Heremans, J. P.; Jovovic, V.; Toberer, E. S.; Saramat, A.; Kurosaki, K.; Charoenphakdee, A.; Yamanaka, S.; Snyder, G. J. Enhancement of Thermoelectric Efficiency in PbTe by Distortion of the Electronic Density of States. *Science* **2008**, *321*, 554–557.

(7) Tan, G.; Zhao, L.-D.; Kanatzidis, M. G. Rationally Designing High-Performance Bulk Thermoelectric Materials. *Chem. Rev.* **2016**, *116*, 12123–12149.

(8) He, Y.; Day, T.; Zhang, T.; Liu, H.; Shi, X.; Chen, L.; Snyder, G. J. High Thermoelectric Performance in Non Toxic Earth Abundant Copper Sulfide. *Adv. Mater.* **2014**, *26*, 3974–3978.

(9) Liu, H.; Shi, X.; Xu, F.; Zhang, L.; Zhang, W.; Chen, L.; Li, Q.; Uher, C.; Day, T.; Snyder, G. J. Copper Ion Liquid-Like Thermoelectrics. *Nat. Mater.* **2012**, *11*, 422 – 425.

(10) Ohtaki, M.; Araki, K.; Yamamoto, K. High Thermoelectric Performance of Dually Doped ZnO Ceramics. *J. Electron. Mater.* **2009**, *38*, 1234–1238.

(11) Chen, X.; Parker, D.; Du, M.-H.; Singh, D. J. Potential Thermoelectric Performance of Hole-Doped Cu_2O. *New J. Phys.* **2013**, *15*, 043029–1–13.

(12) Walia, S.; Balendhran, S.; Nili, H.; Zhuiykov, S.; Rosengarten, G.; Wang, Q. H.; Bhaskaran, M.; Sriram, S.; Strano, M. S.; Kalantar-zadeh, K. Transition Metal Oxides – Thermoelectric Properties. *Progress in Materials Science* **2013**, *58*, 1443 – 1489.

(13) Miller, S. A.; Gorai, P.; Aydemir, U.; Mason, T. O.; Stevanovic, V.; Toberer, E. S.; Snyder, G. J. SnO as a Potential Oxide Thermoelectric Candidate. *J. Mater. Chem. C* **2017**, *5*, 8854–8861.

(14) He, J.; Liu, Y.; Funahashi, R. Oxide Thermoelectrics: The Challenges, Progress, and Outlook. *J. Mater. Res.* **2011**, *26*, 1762–1772.

(15) Ohtaki, M.; Tsubota, T.; Eguchi, K.; Arai, H. High-Temperature Thermoelectric Properties of $Zn_1 - xAl_xO$. *J. Appl. Phys.* **1996**, *79*, 1816–1818.

(16) Tynell, T.; Karppinen, M. ZnO: Hydroquinone Superlattice Structures Fabricated by Atomic/Molecular Layer Deposition. *Thin Solid Films* **2014**, *551*, 23 – 26.

(17) Karttunen, A. J.; Tynell, T.; Karppinen, M. Atomic-Level Structural and Electronic Properties of Hybrid Inorganic–Organic ZnO:Hydroquinone Superlattices Fabricated by ALD/MLD. *J. Phys. Chem. C* **2015**, *119*, 13105–13114.

(18) Karttunen, A. J.; Tynell, T.; Karppinen, M. Layer-By-Layer Design of Nanostructured Thermoelectrics: First-principles Study of ZnO:organic Superlattices Fabricated by ALD/MLD. *Nano Energy* **2016**, *22*, 338 – 348.

(19) Terasaki, I.; Sasago, Y.; Uchinokura, K. Large Thermoelectric Power in $NaCo_2O_4$ Single Crystals. *Phys. Rev. B* **1997**, *56*, R12685–R12687.

(20) Fujita, K.; Mochida, T.; Nakamura, K. High-Temperature Thermoelectric Properties of $Na_xCoO_{2-\delta}$ Single Crystals. *Jpn. J. Appl. Phys.* **2001**, *40*, 4644–4647.

(21) Wan, C.; Gu, X.; Dang, F.; Itoh, T.; Wang, Y.; Sasaki, H.; Kondo, M.; Koga, K.; Yabuki, K.; Snyder, G. J. et al. Flexible n-type Thermoelectric Materials by Organic Intercalation of Layered Transition Metal Dichalcogenide TiS_2. *Nat. Mater.* **2015**, *14*, 622–627.

(22) Voneshen, D. J.; Refson, K.; Borissenko, E.; Krisch, M.; Bosak, A.; Piovano, A.; Cemal, E.; Enderle, M.; Gutmann, M. J.; Hoesch, M. et al. Suppression of Thermal Conductivity by Rattling Modes in Thermoelectric Sodium Cobaltate. *Nat. Mater.* **2013**, *12*, 1028–1032.

(23) Gorai, P.; Stevanović, V.; Toberer, E. S. Computationally Guided Discovery of Thermoelectric Materials. *Nat. Rev. Mats.* **2017**, *2*, 17053–1–16.

(24) Ricci, F.; Chen, W.; Aydemir, U.; Snyder, G. J.; Rignanese, G.-M.; Jain, A.; Hautier, G. An Ab Initio Electronic Transport Database for Inorganic Materials. *Scientific Data* **2017**, *4*, 170085–1–13.

(25) Pei, Y.; Wang, H.; Snyder, G. J. Band Engineering of Thermoelectric Materials. *Adv. Mater.* **2012**, *24*, 6125–6135.

(26) Heremans, J. P.; Wiendlocha, B.; Chamoire, A. M. Resonant Levels in Bulk Thermoelectric Semiconductors. *Energy Environ. Sci.* **2012**, *5*, 5510–5530.

(27) Togo, A.; Chaput, L.; Tanaka, I. Distributions of Phonon Lifetimes in Brillouin Zones. *Phys. Rev. B* **2015**, *91*, 094306–1–31.

(28) Madsen, G. K.; Singh, D. J. BoltzTraP. A Code for Calculating Band-Structure Dependent Quantities. *Comput. Phys. Commun.* **2006**, *175*, 67 – 71.

(29) Sansone, G.; Ferretti, A.; Maschio, L. Ab Initio Electronic Transport and Thermoelectric Properties of Solids from Full and Range-Separated Hybrid Functionals. *J. Chem. Phys.* **2017**, *147*, 114101–1–6.

(30) Ziman, J. M. *Electrons and Phonons: The Theory of Transport Phenomena in Solids*; Oxford University Press, 1960.

(31) Kirtman, B.; Maschio, L.; Rérat, M.; Springborg, M. *Frontiers of Quantum Chemistry*; Springer, 2018; pp 87–115.

(32) Pizzi, G.; Volja, D.; Kozinsky, B.; Fornari, M.; Marzari, N. BoltzWann: A Code for the Evaluation of Thermoelectric and Electronic Transport Properties with a Maximally-Localized Wannier Functions Basis. *Computer Physics Communications* **2014**, *185*, 422–429.

(33) Mustafa, J. I.; Bernardi, M.; Neaton, J. B.; Louie, S. G. Ab Initio Electronic Relaxation Times and Transport in Noble Metals. *Phys. Rev. B* **2016**, *94*, 155105–1–5.

(34) Bernardi, M. First-Principles Dynamics of Electrons and Phonons. *Eur. Phys. J. B* **2016**, *89*, 239–1–15.

(35) Giustino, F. Electron-Phonon Interactions from First Principles. *Rev. Mod. Phys.* **2017**, *89*, 015003–1–63.

(36) Dovesi, R.; Orlando, R.; Erba, A.; Zicovich-Wilson, C. M.; Civalleri, B.; Casassa, S.; Maschio, L.; Ferrabone, M.; De La Pierre, M.; D'Arco, P. et al. CRYSTAL14: A Program for the Ab Initio Investigation of Crystalline Solids. *Int. J. Quantum Chem.* **2014**, *114*, 1287–1317.

(37) Dovesi, R.; Erba, A.; Orlando, R.; Zicovich-Wilson, C. M.; Civalleri, B.; Maschio, L.; Rérat, M.; Casassa, S.; Baima, J.; Salustro, S. et al. Quantum-Mechanical Condensed Matter Simulations with CRYSTAL. *Wiley Interdiscip. Rev. Comput. Mol. Sci.* **2017**, e1360–1–36.

(38) Perdew, J. P.; Burke, K.; Ernzerhof, M. Generalized Gradient Approximation Made Simple. *Phys. Rev. Lett.* **1996**, *77*, 3865–3868.

(39) Adamo, C.; Barone, V. Toward Reliable Density Functional Methods Without Adjustable Parameters: The PBE0 model. *J. Chem. Phys.* **1999**, *110*, 6158–6170.

(40) Weigend, F.; Ahlrichs, R. Balanced Basis Sets of Split Valence, Triple Zeta Valence and Quadruple Zeta Valence Quality for H to Rn: Design and Assessment of Accuracy. *Phys. Chem. Chem. Phys.* **2005**, *7*, 3297–3305.

(41) Kirfel, A.; Eichhorn, K. Accurate Structure Analysis with Synchrotron Radiation. The Electron Density in Al_2O_3 and Cu_2O. *Acta Crystallogr., A.* **1990**, *A46*, 271–284.

(42) Chattopadhyay, T.; McIntyre, G. J.; Brown, P. J.; Forsyth, J. B. Anisotropic Spin Correlations in CuO Above the Néel Temperature. *Physica C* **1990**, *170*, 371–374.

(43) Rödl, C.; Sottile, F.; Reining, L. Quasiparticle Excitations in the Photoemission Spectrum of CuO from First Principles: A *GW* Study. *Phys. Rev. B* **2015**, *91*, 045102–1–13.

(44) Åsbrink, S.; Waskowska, A. CuO: X-ray Single-Crystal Structure Determination at 196 K and Room Temperature. *J. Phys.: Condens. Matter.* **1991**, *3*, 8173–8180.

(45) Kittel, C. *Introduction to Solid State Physics*, 8th ed.; John Wiley & Sons, Inc.: Hoboken, NJ, 2005.

(46) Sasaki, S.; Fujino, K.; Takeuchi, Y. X-Ray Determination of Electron-Density Distributions in Oxides, MgO, MnO, CoO, and NiO, and Atomic Scattering Factors of Their Constituent Atoms. *Proc. Japan Acad. Ser. B* **1979**, *55*, 43–48.

(47) Cheetham, A. K.; Hope, D. A. O. Magnetic Ordering and Exchange Effects in the Antiferromagnetic Solid Solutions $Mn_xNi_{1-x}O$. *Phys. Rev. B* **1983**, *27*, 6964–6967.

(48) Fernandez, V.; Vettier, C.; de Bergevin, F.; Giles, C.; Neubeck, W. Observation of Orbital Moment in NiO. *Phys. Rev. B* **1998**, *57*, 7870–7876.

(49) Kwon, S. K.; Min, B. I. Unquenched Large Orbital Magnetic Moment in NiO. *Phys. Rev. B* **2000**, *62*, 73–75.

(50) Yang, B. X.; Tranquada, J. M.; Shirane, G. Neutron Scattering Studies of the Magnetic Structure of Cupric Oxide. *Phys. Rev. B* **1988**, *38*, 174–178.

(51) Yang, B. X.; Thurston, T. R.; Tranquada, J. M.; Shirane, G. Magnetic Neutron Scattering Study of Single-Crystal Cupric Oxide. *Phys. Rev. B* **1989**, *39*, 4343–4349.

(52) Baumeister, P. W. Optical Absorption of Cuprous Oxide. *Phys. Rev.* **1961**, *121*, 359 – 362.

(53) Önsten, A.; Månsson, M.; Claesson, T.; Muro, T.; Matsushita, T.; Nakamura, T.; Kinoshita, T.; Karlsson, U. O.; Tjernberg, O. Probing the Valence Band Structure of

Cu_2O Using High-Energy Angle-Resolved Photoelectron Spectroscopy. *Phys. Rev. B* **2007**, *76*, 115127–1–7.

(54) Linnera, J.; Karttunen, A. J. Ab Initio Study of the Lattice Thermal Conductivity of Cu_2O Using the Generalized Gradient Approximation and Hybrid Density Functional Methods. *Phys. Rev. B* **2017**, *96*, 014304–1–12.

(55) Marabelli, F.; Parravicini, G. B.; Salghetti-Drioli, F. Optical Gap of CuO. *Phys. Rev. B* **1995**, *52*, 1433–1436.

(56) Ghijsen, J.; Tjeng, L. H.; van Elp, J.; Eskes, H.; Westerink, J.; Sawatzky, G. A.; Czyzyk, M. T. Electronic Structure of Cu_2O and CuO. *Phys. Rev. B* **1988**, *38*, 11322–11330.

(57) Ray, S. C. Preparation of Copper Oxide Thin Film by the Sol–Gel-like Dip Technique and Study of Their Structural and Optical Properties. *Sol. Energ. Mat. Sol. Cells* **2001**, *68*, 307 – 312.

(58) Tahir, D.; Tougaard, S. Electronic and Optical Properties of Cu, CuO and Cu_2O Studied by Electron Spectroscopy. *J. Phys.: Condens. Matter.* **2012**, *24*, 175002–1–8.

(59) Rocquefelte, X.; Whangbo, M.-H.; Villesuzanne, A.; Jobic, S.; Tran, F.; Schwarz, K.; Blaha, P. Short-Range Magnetic Order and Temperature-Dependent Properties of Cupric Oxide. *J. Phys.: Condens. Matter.* **2010**, *22*, 045502–1–7.

(60) Heinemann, M.; Eifert, B.; Heiliger, C. Band Structure and Phase Stability of the Copper Oxides Cu_2O, CuO, and Cu_4O_3. *Phys. Rev. B* **2013**, *87*, 115111–1–5.

(61) Wang, Y.; Lany, S.; Ghanbaja, J.; Fagot-Revurat, Y.; Chen, Y. P.; Soldera, F.; Horwat, D.; Mücklich, F.; Pierson, J. F. Electronic Structures of Cu_2O, Cu_4O_3, and CuO: A Joint Experimental and Theoretical Study. *Phys. Rev. B* **2016**, *94*, 245418–1–10.

(62) Fujimori, A.; Minami, F. Valence-Band Photoemission and Optical Absorption in Nickel Compounds. *Phys. Rev. B* **1984**, *30*, 957–971.

(63) Hüfner, S.; Osterwalder, J.; Riesterer, T.; Hulliger, F. Photoemission and Inverse Photoemission Spectroscopy of NiO. *Solid State Commun.* **1984**, *52*, 793 – 796.

(64) de P. R. Moreira, I.; Illas, F.; Martin, R. L. Effect of Fock Exchange on the Electronic Structure and Magnetic Coupling in NiO. *Phys. Rev. B* **2002**, *65*, 155102–1–14.

(65) Setyawan, W.; Curtarolo, S. High-Throughput Electronic Band Structure Calculations: Challenges and Tools. *Comput. Mater. Sci.* **2010**, *49*, 299 – 312.

(66) von Bädeker, K. Über die Elektrische Leitfähigkeit und die Thermoelektrische Kraft einiger Schwermetallverbindungen. *Ann. Phys.* **1907**, *327*, 749–766.

(67) Mönch, G. Zur Theorie der Thermospannungen zwischen Halbleiter und Metall auf Grund der Fermischen Statistik. *Z. Phys.* **1933**, *83*, 247–252.

(68) Greenwood, N.; Anderson, J. Conductivity and Thermo-Electric Effect in Cuprous Oxide. *Nature* **1949**, *164*, 346–347.

(69) Zirin, M. H.; Trivich, D. Thermoelectric Effect in Single Crystal Cuprous Oxide at High Temperatures. *J. Chem. Phys.* **1963**, *39*, 870–875.

(70) Young, A.; Schwartz, C. Electrical Conductivity and Thermoelectric Power of Cu_2O. *J. Phys. Chem. Solids* **1969**, *30*, 249 – 252.

(71) Hartung, D.; Gather, F.; Hering, P.; Kandzia, C.; Reppin, D.; Polity, A.; Meyer, B. K.; Klar, P. J. Assessing the Thermoelectric Properties of Cu_xO (x = 1 to 2) Thin Films as a Function of Composition. *Appl. Phys. Lett.* **2015**, *106*, 253901–1–5.

(72) Figueira, J.; Loureiro, J.; Marques, J.; Bianchi, C.; Duarte, P.; Ruoho, M.; Tittonen, I.; Ferreira, I. Optimization of Cuprous Oxides Thin Films to be used as Thermoelectric Touch Detectors. *ACS Appl. Mater. Interfaces* **2017**, *9*, 6520–6529.

(73) O'Keeffe, M.; Moore, W. J. Electrical Conductivity of Monocrystalline Cuprous Oxide. *J. Chem. Phys.* **1961**, *35*, 1324–1328.

(74) Fortin, E.; Weichman, F. L. Hall Effect and Electrical Conductivity of Cu_2O Monocrystals. *Can. J. Phys.* **1966**, *44*, 1551–1561.

(75) Jeong, Y. K.; Choi, G. M. Nonstoichiometry and Electrical Conduction of CuO. *J. Chem. Phys. Solids* **1996**, *57*, 81–84.

(76) Keem, J.; Honig, J. Selected Electrical and Thermal Properties of Undoped Nickel Oxide. *Defense Technical Information Center* **1978**,

(77) Parravano, G. Thermoelectric Behavior of Nickel Oxide. *J. Chem. Phys.* **1955**, *23*, 5–10.

(78) Nachman, M.; Cojocaru, L.; Ribco, L. Electrical Properties of Non-Stoichiometric Nickel Oxide. *Phys. Status Solidi B* **1965**, *8*, 773–783.

(79) Shin, W.; Murayama, N. Li-Doped Nickel Oxide as a Thermoelectric Material. *Jpn. J. Appl. Phys.* **1999**, *38*, L1336–L1338.

Graphical TOC Entry